Smoothing Filter-Based Panchromatic Spectral Decomposition for Multispectral and Hyperspectral Image Pansharpening

Mi Wang, Guangqi Xie, *Graduate Student Member, IEEE*, Zhiqi Zhang, Yan Wang, Shao Xiang, and Yingdong Pi

***Abstract*—This article proposes an efficient and high-fidelity panchromatic (PAN) spectral decomposition method based on smoothing filtering for multispectral (MS) and hyperspectral (HS) image pansharpening. The proposed method assumes that the high-frequency spatial details at the same scale are the same for different spectral images captured by the satellite at the same time. When the PAN image is prefiltered and down-sampled to the MS scale, it will have the same high-frequency spatial detail as the MS image, with only low-frequency spectral differences. Prefiltering for antialiasing when downsampling. Then, the spectral decomposition coefficients from down-sampled PAN image to MS image can be calculated on MS scale. The low-frequency spectral information of an image at different scales is the same, the spectral decomposition coefficients on the MS scale can be up-sampled to the PAN scale, and the original PAN image can be spectrally decomposed to obtain the sharpened image. The proposed method only decomposes the low-frequency spectrum, and the high-frequency spatial details are the same as the original PAN image, the spatial detail is well preserved. This article verifies the effect of the proposed method on MS and HS image sharpening through experiments, and the results show that the proposed method is better than the comparison method. This article also controls other variables to compare with the HPM method. The results show that the hybrid quality with no reference and spatial distortion index (D_s) of the proposed method are better than the HPM method.**

***Index Terms*—Hyperspectral (HS), multispectral (MS), pansharpening, spectral decomposition.**

Manuscript received December 16, 2021; revised February 8, 2022 and March 20, 2022; accepted April 15, 2022. Date of publication April 26, 2022; date of current version May 16, 2022. This work was supported in part by the IEEE Publication Technology Group, in part by the National Natural Science Foundation of China under Grant 61825103, Grant 91838303, Grant 61901307, Grant 91638301, and Grant 91738302, in part by the Open Research Fund of the State Key Laboratory of Information Engineering in Surveying, Mapping and Remote Sensing, Wuhan University, under Grant 20E01, in part by the Key Research and Development Plan Project of Hubei Province under Grant 2020BIB006, in part by the Key Project of Hubei Provincial Natural Science Foundation under Grant 2020CFA001, and in part by the Major Program of National Natural Science Foundation of China under Grant 42192583. *(Corresponding author: Guangqi Xie.)*

Mi Wang, Guangqi Xie, Shao Xiang, and Yingdong Pi are with the State Key Laboratory of Information Engineering in Surveying, Mapping, and Remote Sensing, Wuhan University, Wuhan 430079, China (e-mail: wangmi@whu.edu.cn; xiegqrs@whu.edu.cn; xiangshao@whu.edu.cn; pyd_imars@whu.edu.cn).

Zhiqi Zhang is with the School of Computer Science, Hubei University of Technology, Wuhan 430068, China (e-mail: zzq540@hbut.edu.cn).

Yan Wang is with the Institute of Beijing Remote Sensing Information, Beijing 100871, China (e-mail: 13146642672@126.com).

Digital Object Identifier 10.1109/JSTARS.2022.3170488

I. Introduction

PANSHARPENING fuses multispectral (MS) and panchromatic (PAN) images, which has been an active research field for the last decades [1]–[3]. In recent years, with the fast development of hyperspectral (HS) satellites, HS pansharpening, which pansharpens HS images, also attracts great attention [4]–[6]. Both MS and HS pansharpening[1] by taking advantages from high-spectral- but low-spatial-resolution MS/HS images and high-spatial-resolution PAN images aim at achieving images with both high spatial and spectral resolutions to meet the demands of applications, such as classification, target detection, scene interpretation, and spectral unmixing [7], [8].

Classical pansharpening methods can be roughly grouped into two categories: based on component substitution (CS) and multiresolution analysis (MRA) [1], [3], [7]. On the one hand, CS-based methods substitute the components of a high-spectral-resolution image by those of a PAN image, such as methods based on principal component analysis (PCA) [9]–[11], Brovey transform (BT) [12], [13], and Gram–Schmidt (GS) transform [14], [15], and these methods transform a low-spatial-resolution image into another domain and then replace the main component by the spatial details from the PAN image. On the other hand, MRA-based approaches, such as approaches based on decimated wavelet transform [16], smoothing-filter-based intensity modulation (SFIM) [17], high-pass filtering (HPF) [18], morphological filtering [19], [20], and Laplacian pyramid [21], [22], involve multiresolution decomposition to extract the spatial details from a PAN image [7].

Recently, deep learning (DL) technology predominates image sharpening, and it can be mainly divided into two categories: One is to fit the sharpened image model by minimizing the cost function [23]–[25], and the other is to simulate the sharpened image through the generative adversarial network (GAN) [26]–[28]. However, these two methods will face the same problem, i.e., there are no real training data. Only simulated data can be used for training, and when they are used in real scenes, the effect and versatility are not particularly good. Moreover, the amount of real remote sensing image data is extremely large, and it is difficult for DL methods to achieve the efficiency of traditional methods. The current mainstream DL methods are processed

[1]For simplicity, we use pansharpening for both MS and HS pansharpening.

in blocks in pansharpening, such as 256×256. In a published paper [29], the processing time for a single block was about 1 s. For submeter high-resolution optical satellites, the number of pixels in a single scene can reach about 60000×60000. Even if the overlap between blocks was not considered, the number of blocks to be calculated was about 55 000, i.e., 55 000 s or about 15 h; obviously, such a large computing time does not meet the needs of engineering operation. However, the DL method is very promising and can overcome the problems of poor effect, efficiency, and versatility in real scenarios in the future.

Although the aforementioned methods are basically for MS image sharpening, some of them can be directly introduced into HS image sharpening, such as SFIM, GS, and PCA. There are also some methods for HS image sharpening, such as Bayesian fusion [30] and HySure fusion [31], [32]. These methods have also achieved good results, but their versatility is relatively weak.

In summary, the CS method cannot handle a single band, the calculation efficiency is low, and the color cast is serious. Also, the MRA method has low image clarity, and the modulation transfer function (MTF) calculation of the MTF method is difficult. Moreover, the DL method is currently poor in practicability. Therefore, this article proposes a smoothing-filter-based panchromatic spectral decomposition (SFPSD) for MS and HS image pansharpening. This method has a wide range of applications, high calculation efficiency, and easy engineering and is suitable for sharpening MS and HS images.

II. Methodology

Let $\mathbf{P} \in \mathbb{R}^{H \times W}$ denote an observed PAN image with size $H \times W$, let $\mathbf{M} \in \mathbb{R}^{h \times w \times N_b}$ denote an observed MHS image (with N_b being the number of bands), let $\widetilde{\mathbf{M}} \in \mathbb{R}^{H \times W \times N_b}$ be a preinterpolated LRMHS, which has been interpolated spatially to the scale of the PAN image, and let $\widehat{\mathbf{M}}$ be the pansharpened HRMHS image. $\mathbf{M}_b$, $\widehat{\mathbf{M}}_b$, and $\widetilde{\mathbf{M}}_b$ are the bth bands of $\mathbf{M}$, $\widehat{\mathbf{M}}$, and $\widetilde{\mathbf{M}}$, respectively. $\mathbf{P}_L$ is the preinterpolated LRPAN image, which has been low-pass filtered and interpolated spatially to the scale of the MHS image.

A. Theory

Proposed method has two following assumptions.

1) There are only low-frequency spectral differences but no high-frequency spatial differences between the same scale images, which be taken by satellite at the same time and area.
2) There are only high-frequency spatial differences at different scales of an image, but no low-frequency spectral differences.

The PAN and the MHS images can be considered as taken at the same time and area. According to assumption 1, when the original PAN images are prefiltered and down-sampled to the MHS scale, the high-frequency spatial details of the down-sampled PAN images can be considered to be the same as the MHS images. There are only low-frequency spectral differences between them. Prefiltering is for antialiasing in downsampling. At this scale, the formula for the MHS bth band image and the PAN image can be defined as follows:

$$\mathbf{M}_b = f_L^{(b)}(\mathbf{P}_L) \tag{1}$$

The $f_L^{(b)}(\cdot)$ is the spectral decomposition function on the MHS scale. Define this function as a linear function

$$\mathbf{M}_b = \mathbf{P}_L \bullet \rho_L^{(b)} \tag{2}$$

In the above formula, $\rho_L^{(b)}$ is defined as the spectral decomposition coefficients of $\mathbf{P}_L$ to $\mathbf{M}_b$.

The spectral decomposition coefficients $\rho_L^{(b)}$ of the $\mathbf{P}_L$ can be calculated as follows:

$$\rho_L^{(b)} = \frac{\mathbf{M}_b}{\mathbf{P}_L} \tag{3}$$

The spectral decomposition coefficients on the MHS scale can be used to decompose the original image on the PAN scale to obtain a sharpened image according to Assumption 2.

Therefore, the decomposition coefficients of the PAN spectrum can be interpolated by $\rho_L^{(b)}$, which will be defined as $\rho^{(b)}$.

The sharpened MHS bth band image can be defined as follows:

$$\widehat{\mathbf{M}}_b = f^{(b)}(\mathbf{P}) = \mathbf{P} \bullet \rho^{(\mathbf{b})}. \tag{4}$$

B. Method

Based on the aforementioned theory, this article proposes the SFPSD algorithm to pansharpen the MHS images. The algorithm is described in Algorithm 1.

Algorithm 1: SFPSD.

INPUT: Registered $\mathbf{P}$ and $\mathbf{M}$.
OUTPUT: $\widehat{\mathbf{M}}$.
$[H, W, N_b] = \text{size}(\mathbf{M})$;
For b **in** range(N_b):
Step 1: Enhance $\mathbf{P}$, make $\mathbf{P}$ distribution consistent with $\mathbf{M}_b$ in bth bands: $\mathbf{P}_E^{(b)}$;
Step 2: Low-pass filter $\mathbf{P}$ and downsample fuzzy $\mathbf{P}$ to MHS image scale: $\mathbf{P}_{EL}^{(b)}$;
Step 3: Calculate the panchromatic decomposition coefficients: $\rho_L^{(b)} = \mathbf{M}_b / \mathbf{P}_{EL}^{(b)}$;
Step 4: Upsampled panchromatic decomposition coefficients to PAN image resolution: $\rho^{(b)}$;
Step 5: Calculate the decomposition value of the bth band: $\widehat{\mathbf{M}}_b = \mathbf{P}_E^{(b)} * \rho^{(b)}$;
End for;
Output $\widehat{\mathbf{M}}$.

Step 1 in Algorithm 1 enhances the PAN image to make the distribution of PAN and MHS images consistent, which is particularly critical when the initial distributions of the two differ greatly. It is not a necessary step when the two distributions are basically the same. This step is calculated as follows:

$$\mathbf{P}_E^{(b)} = (\mathbf{P} - \text{mean}(\mathbf{P})) \frac{\text{std}(\mathbf{M}_b)}{\text{std}(\mathbf{P})} + \text{mean}(\mathbf{M}_b) \tag{5}$$

In (5), $\mathbf{P}_E^{(b)}$ is the corresponding enhanced PAN image of the bth band of the MHS image, $mean(\mathbf{P})$ is the mean value of the PAN image, $std(\mathbf{P})$ is the standard deviation value of the PAN image, $mean(\mathbf{M}_b)$ is the mean value of the bth band of the MHS image, and $std(\mathbf{M}_b)$ is the standard deviation value of the bth band of the MHS image.

The purpose of Step 2 in Algorithm 1 is to obtain $\mathbf{P}_{\mathrm{EL}}^{(b)}$ whose definition and resolution are consistent with those of the bth MHS images. It low-pass filters the bth enhanced PAN image and downsamples the fuzzy image into an MHS image resolution. This step will filter out the high-frequency part of the enhanced PAN image and only keep its low-frequency part. It can be performed in the frequency domain by wavelet transform or in the spatial domain by Gaussian pyramids.

Step 3 in Algorithm 1 calculated the PAN decomposition coefficients, as in the following:

$$\rho_L^{(b)} = \frac{\mathbf{M}_b}{\mathbf{P}_{EL}^{(b)}} \tag{6}$$

Step 4 in Algorithm 1 upsamples the PAN decomposition coefficients $\rho_L^{(b)}$ into a PAN image resolution: $\rho^{(b)}$.

Step 5 in Algorithm 1 decomposes the enhanced PAN image to obtain the bth sharpened MHS image

$$\widehat{\mathbf{M}}_b = \mathbf{P}_E^{(b)} * \rho^{(b)} \tag{7}$$

It can be seen from the calculation steps that the algorithm in this article is not limited by the number of MHS image bands, and even single-band sharpening can also be supported.

C. Quality Indices

To objectively evaluate the performance of this algorithm, this study evaluates the effect of pansharpening from the following indicators. These indicators will objectively evaluate the results from the spectral, spatial, and global perspectives. In addition, the accuracy evaluation will be carried out from two aspects: reduced-resolution assessment and full-resolution assessment.

1) Reduced-Resolution Assessment With Reference: Reduced-resolution assessment synthetically generates simulated observed images from a reference MHS image and then evaluates the result of the method against that reference image. The indicators are as follows.

(1) Cross correlation

Cross correlation (CC) characterizes the geometric distortion, which is defined as

$$CC\left(\widehat{M}, M\right) = \frac{1}{N_b}\sum_{b=1}^{N_b} \mathrm{CCS}(\widehat{M}_b, M_b) \tag{8}$$

where CCS is the cross correlation for a single-band image, which is defined as

$$\mathrm{CCS}(A,B) = \frac{\sum_{j=1}^{n}(A_j-\mu_A)(B_j-\mu_B)}{\sqrt{\sum_{j=1}^{n}(A_j-\mu_A)^2\sum_{j=1}^{n}(B_j-\mu_B)^2}} \tag{9}$$

where $n = H * W$ and $\mu_A = (\frac{1}{n})\sum_{j=1}^{n} A_j$ is the sample mean of A. The ideal value of CC is one.

(2) Spectral angle mapper

The spectral angle mapper (SAM) is a spectral measure, which is defined as

$$\mathrm{SAM}\left(\widehat{M}, M\right) = \frac{1}{n}\sum_{j=1}^{n}\arccos\left(\frac{\left(\widehat{M}, M\right)}{||\widehat{M}_j|| \bullet ||M_j||}\right) \tag{10}$$

where $(\widehat{M}, M) = \widehat{M}_j{}^{\mathrm{T}} M_j$ is the inner product between $\widehat{M}_j$ and M_j at the jth pixel and $||.||$ is the L_2 norm. SAM is a measure of spectral shape preservation, and its ideal value is zero.

(3) Root-mean-square error

The root-mean-square error ($RMSE$) measures the L_2 error between the two matrices $\widehat{M}$ and M

$$\mathrm{RMSE}\left(\widehat{M}, M\right) = \frac{||\widehat{M} - M||_F}{\sqrt{n * N_b}} \tag{11}$$

where $||.||_F$ is the Frobenius norm. The ideal value of RMSE is zero.

(4) Erreur relative globale adimensionnelle de synthese

The erreur relative globale adimensionnelle de synthese ($ERGAS$) offers a global indication of the quality of a fused image. It is defined as

$$\mathrm{ERGAS}\left(\widehat{M}, M\right) = 100d\sqrt{\frac{1}{N_b}\sum_{b=1}^{N_b}\left(\frac{\mathrm{RMSE}_b}{\mu_b}\right)^2} \tag{12}$$

where d is the ratio between the linear resolutions of the PAN and MHS images. The ideal value of $ERGAS$ is zero.

2) Full-Resolution Assessment With No Reference: Full-resolution assessment infers the quality of the pansharpened image at the resolution of the PAN image without resorting to a single reference image. It will be evaluated by true observed images.

(1) Spectral distortion index

The spectral distortion index D_λ from the Khan protocol [33] is defined as

$$D_\lambda = 1 - Q2^n(\widehat{M}, \widetilde{M}) \tag{13}$$

Because the MTF is generally not public and will also change with time, the filter uses a Gaussian pyramid, which is different from [2].

$Q2^n$ is the multiband extension of the universal image quality index and was introduced for quality assessment of the pansharpened MS image, first for four bands and later extended to 2^n bands [34]–[36]. Each pixel of an image with N spectral bands is accommodated into a hypercomplex (HC) number with one real part and $N-1$ imaginary parts.

Let $z = z(c,r)$ and $\hat{z} = \hat{z}(c,r)$ denote the HC representations of the reference and test spectral vectors at pixel (c,r), respectively. $Q2^n$ is defined as

$$Q2^n = \frac{|\sigma_{z\hat{z}}|}{\sigma_z\sigma_{\hat{z}}} \bullet \frac{2\sigma_z\sigma_{\hat{z}}}{{\sigma_z}^2 + {\sigma_{\hat{z}}}^2} \bullet \frac{2\,|\bar{z}|\,|\bar{\hat{z}}|}{|\bar{z}|^2 + |\bar{\hat{z}}|^{2}}. \tag{14}$$

(2) Spatial distortion index

The spatial distortion index is defined as

$$D_s = \sqrt[q]{\left|Q\left(I_{\widehat{M}}, \mathbf{P}\right) - Q\left(I_M, \mathbf{P}_L\right)\right|^q} \tag{15}$$

TABLE I
INTRODUCTION OF DATA

Satellites	Parameters	Description		Satellites	Parameters	Description	
GF-7	Spectral range	PAN	$0.45-0.90\mu$m	ZY-1E	Spectral range	HS (VNIR)	$0.4-1.05\mu\text{m}, 76bands/10n\text{m}$
		MS	$0.45-0.52\mu$m $0.52-0.59\mu$m $0.63-0.69\mu$m $0.76-0.89\mu$m			HS (SWIR)	$1.05-2.5\mu\text{m}, 90bands/20n\text{m}$
	Spatial resolution	PAN	0.8m		Spatial resolution	HS	30m
		MS	3.2m			/	/

where $Q = Q2^0$ and $I_{\widehat{M}}$ and I_M are the intensities of $\widehat{M}$ and M, respectively, which are defined as

$$I_{\widehat{M}} = \frac{1}{N_b}\sum_{b=1}^{N_b}\widehat{M}_b, I_M = \frac{1}{N_b}\sum_{b=1}^{N_b}M_b \tag{16}$$

(3) Hybrid quality with no reference

The hybrid quality with no reference [37] ($HQNR$) borrows the spatial distortion index D_s from QNR and the spectral distortion index D_λ from the Khan protocol. It is defined as

$$\text{HQNR} = (1-D_\lambda)^\alpha(1-D_s)^\beta \tag{17}$$

where usually $\alpha = \beta = 1$.

III. DATA INTRODUCTION

The data used in this study include those of the GaoFen-7 (GF-7) satellite in the series of high-resolution Earth observation satellites planned by China's "China High-resolution Earth Observation System" and those of the ZiYuan-1E (ZY-1E) satellite of the National Land Satellite Remote Sensing Application Center of the Ministry of Natural Resources. The selected images include various topography and landforms such as mountains, plains, and coastal areas. The detailed data usage is shown in Table I.

IV. RESULTS AND DISCUSSION

To verify the effect of the proposed algorithm, the performance with reference for the HS image and the performance without reference for the MS image were tested. The comparison method in this article refers to the MATLAB ToolBox [2], [38]–[40], and the comparative methods are described as follows.

1) GT: Ground real images, only in the reduced resolution assessment with reference mode.
2) EXP: MHS image interpolation, using the built-in interpolation function of MATLAB [41].
3) SFIM: Smoothing filter-based intensity modulation (SFIM) [17].
4) Brovey: BT for image fusion [12], [13].
5) HPF: High-pass filtering for image fusion [18].
6) MTF-GLP: Generalized laplacian pyramid (GLP) [42] with MTF-matched filter [19] with unitary injection model.
7) MTF-GLP-FS: GLP with MTF-matched filter and a new full resolution regression-based injection model [43].
8) MTF-GLP-HPM: GLP with MTF-matched filter and multiplicative injection model [44].
9) MTF-GLP-HPM-Haze-min: Gaussian Laplacian pyramid with high pass modulation injection model haze corrected [45].
10) MTF-GLP-HPM-R: A regression-based high-pass modulation pansharpening approach [46].
11) MF_HG_Pansharpen: Morphological pyramid decomposition using half-gradient [20].
12) BDSD-PC: Band-dependent spatial-detail (BDSD) model solving an optimization constrained problem [47].
13) GS: Gram Schmidt [14].
14) GSA: Gram Schmidt Adaptive [48].
15) GS_Segm_GSA: Segmentation-based version of the GS Adaptive algorithm [49].
16) GS_Segm_GS2GLP: Segmentation-based version of the GS algorithm with GLP [49].
17) Bayesian_Naive: Bayesian fusion of HS images [30].
18) HySure: Fuse HS remote sensing images with either MS or PAN ones [31], [32].

The low-pass filter of the proposed method (Step 4 in Algorithm 1) in this experiment used a Gaussian pyramid. The registration accuracy of the PAN and MHS images has a great influence on the fusion effect [50], [51], so this study chose the method [52] to preprocess the image registration. The experiments were implemented in MATLAB R2020b on a server with an Intel I7-6700 K CPU at 4.0 GHz and a 64-GB RAM.

A. Reduced Resolution Assessment With Reference

Reduced-resolution assessment with reference takes the actual observed HS image as the pansharpened image and simulates the corresponding PAN and HS image fusion to evaluate its effect. The protocol consists of the following steps.

1) Given an HS image as a ground true fused image $\mathbf{GT}$, a simulated observed low-spatial-resolution HS image $\mathbf{M}$ is obtained by applying Gaussian blurring and downsampling to the ground true fused image by ratio R.
2) A simulated PAN image $\mathbf{PAN}$ is obtained by multiplying the reference HS image without the true PAN image by a suitably chosen spectral response vector, i.e., $\mathbf{PAN} = \mathbf{r^T GT}$.
3) The pansharpening method to be evaluated is applied to the simulated observations mhs and pan, which yields an estimated super-resolution HS image $\widehat{\mathbf{M}}$.
4) Finally, the estimated super-resolution HS image and the reference image are compared to obtain quantitative quality measures.

In this section, the ZY-1E 166-band HS data with the spatial size of 1024×1024 from the data introduced in section III are

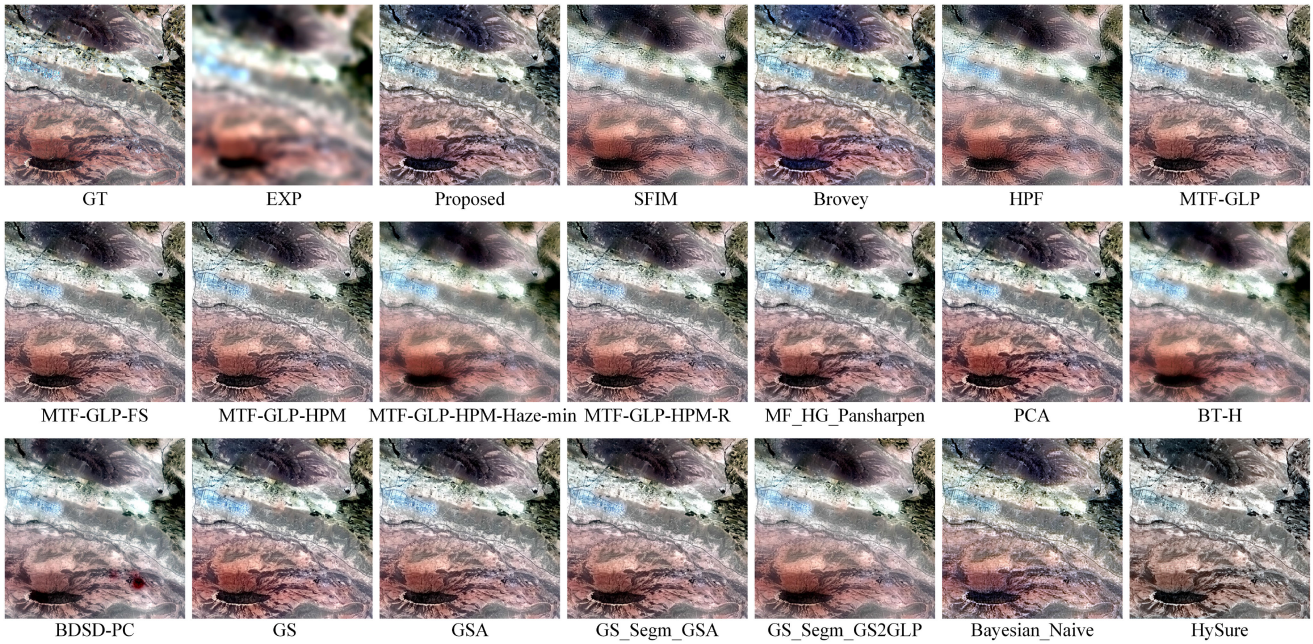

Fig. 1. ZY-1E color image with bands 25, 16, and 8 as RGB in ratio $R = 16$ for different methods.

selected to verify the performance of the algorithm in this article on HS images with the ratio $R = 16$. This study compared the proposed algorithm with 18 common image fusion algorithms. Fig. 1 shows the comparison between the fusion images of the different methods and the ground true image. Each image is displayed as a color image with bands 25, 16, and 8 as RGB, because of ZY-1E's spectral range. It can be seen from the figure that the result of the proposed method is closest to the visual effect of the ground true image. Some methods also have good visual effects, such as Brovey, PCA, and the GS series methods. However, there are some methods that have serious loss of information, such as SFIM, HPF, and BT-H. The proposed method can retain not only the spatial information, but also the color information.

The evaluation indices used are CC, $RMSE$, SAM, and $ERGAS$, which are introduced in Section II. The quantitative evaluation results are shown in Table II. As can be seen from the table, the proposed method has obvious advantages over the other methods for $RMSE$, which is the most important evaluation index in the reduced-resolution assessment with reference. This shows that the difference between the fusion results of the proposed method and the ground true image is the smallest, which is obviously better than the other methods. For the other evaluation indicators, although the proposed method did not achieve the best results, the gap compared with the best results is not particularly obvious. In addition, the proposed method consumes less time in all methods, indicating that it has higher computational efficiency and is suitable for business operation.

TABLE II
EVALUATION INDEX IN RATIO $R = 16$ FOR ZY-1E IMAGE SHARPENING

Name	CC	RMSE	SAM	ERGAS	time/s
GT	1	0	0	0	0
EXP	0.804	146.341	1.746	0.667	0.451
Proposed	0.930	**63.864**	1.747	0.418	2.435
SFIM	0.897	275.206	1.660	40.451	4.186
Brovey	0.926	87.404	1.746	0.475	**0.389**
HPF	0.908	94.155	1.629	0.496	4.323
MTF-GLP	0.929	102.498	1.581	0.525	20.258
MTF-GLP-FS	0.931	99.955	1.622	0.489	13.463
MTF-GLP-HPM	0.914	1733.013	1.635	174.195	20.245
MTF-GLP-HPM-Haze-min	0.897	108.061	1.725	0.518	21.286
MTF-GLP-HPM-R	0.929	103.832	1.659	0.499	12.434
MF_HG_Pansharpen	0.915	88.334	1.622	8.272	23.522
PCA	0.938	84.464	1.628	0.460	9.412
BT-H	0.902	104.061	1.710	0.506	9.915
BDSD-PC	0.930	179.677	1.837	0.733	107.002
GS	0.941	83.574	1.614	0.457	5.838
GSA	0.936	68.683	**1.555**	**0.415**	6.993
GS_Segm_GSA	**0.943**	85.661	1.571	0.447	41.860
GS_Segm_GS2GLP	0.925	96.828	1.608	0.486	67.379
Bayesian_Naive	0.910	77.054	1.783	0.469	3.361
HySure	0.899	71.741	2.169	0.580	386.617

B. Full-Resolution Assessment With No Reference

In this section, the real PAN MS data are mainly used to verify the performance of the algorithm in the MS image sharpening without reference. The test data used are from the GF-7 data with the spatial size of 4096×4096 introduced in Section III. Fig. 2 shows the comparison of the fusion results of the different methods. It can be seen from the figure that, except for some methods that have serious color casts, most of the methods can maintain good fusion colors. Also, it can be clearly seen that the color of the proposed algorithm is maintained well.

To compare the advantages and disadvantages of the proposed method and the other methods in more detail, this article enlarges some of the details in Fig. 2, as shown in Fig. 3. It can be seen from the enlarged detail view that the spatial and spectral information of the proposed method can be maintained well. It can improve the clarity while retaining the spectrum information

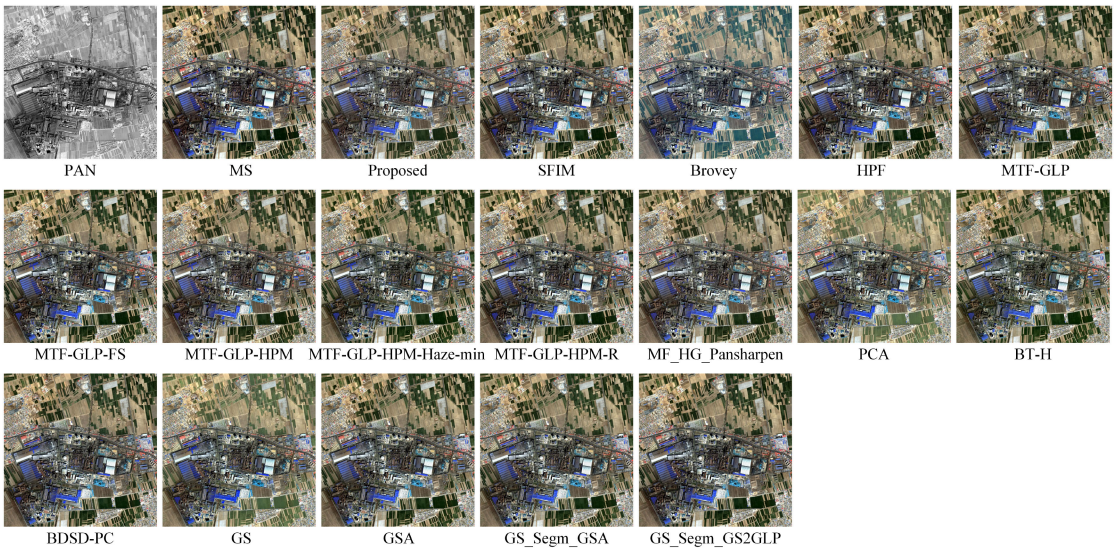

Fig. 2. GF-7 color image with bands 3, 2, and 1 as RGB of different methods.

TABLE III
EVALUATION INDEX FOR GF-7 IMAGE SHARPENING OF DIFFERENT METHODS

Name	*HQNR*	D_λ	D_s	Time/s
EXP	0.858	0.053	0.094	**0.198**
Proposed	**0.950**	**0.022**	0.029	1.409
SFIM	0.949	0.039	0.012	2.840
Brovey	0.795	0.139	0.077	0.294
HPF	0.950	0.040	**0.010**	2.813
MTF-GLP	0.938	0.033	0.030	10.631
MTF-GLP-FS	0.943	0.036	0.021	7.645
MTF-GLP-HPM	0.939	0.032	0.030	10.571
MTF-GLP-HPM-Haze-min	0.945	0.036	0.020	9.620
MTF-GLP-HPM-R	0.944	0.036	0.021	6.863
MF_HG_Pansharpen	0.942	0.030	0.029	6.388
PCA	0.789	0.151	0.070	2.586
BT-H	0.932	0.037	0.033	3.345
BDSD-PC	0.936	0.032	0.034	2.982
GS	0.798	0.136	0.077	3.889
GSA	0.927	0.037	0.037	9.217
GS_Segm_GSA	0.931	0.036	0.034	104.549
GS_Segm_GS2GLP	0.948	0.037	0.016	117.696

to the greatest extent. The proposed method performs most prominently among all the comparison algorithms.

This study used the evaluation index without reference to objectively evaluate the aforementioned fusion results. The evaluation indices without reference are D_λ, D_s, and $HQNR$, which are introduced in Section II. Table III shows the detailed results of the no-reference evaluation indices of the different methods. It can be seen from the table that the proposed method achieves the best results for the $HQNR$ comprehensive index and the spectral distortion index D_λ. Also, the gap between the spatial distortion index D_s and the optimal result is not very obvious. However, the operating efficiency is higher than those of the mainstream fusion methods, and the difference in the fusion effect of some of the best fusion methods on the GF-7 PAN and MS images is not particularly obvious, which can also be seen in Figs. 2 and 3.

In summary, the proposed method can have a better effect on both spatial information and spectral information, which is compared with the current mainstream PAN and MS fusion methods.

C. Discussion

The proposed method belongs to the MRA method, but it has certain characteristics compared with a traditional fusion method. First, the PAN decomposition coefficients of the proposed method is continuous. Second, it has better robustness to the correlation between PAN and MHS images. Finally, it has good performance under large resolution differences. This section will discuss these three aspects as follows.

1) Continuity of PAN Decomposition Coefficients: The classical SFIM technique [17] is defined as follows:

$$\mathrm{DN}(\lambda)_{\mathrm{sim}} = \frac{\mathrm{DN}(\lambda)_{\mathrm{low}}\mathrm{DN}(\lambda)_{\mathrm{high}}}{\mathrm{DN}(\lambda)_{\mathrm{mean}}} \tag{18}$$

where $DN(\lambda)_{\mathrm{sim}}$ is the simulated higher resolution pixel corresponding to $DN(\lambda)_{\mathrm{low}}$ and $DN(\lambda)_{\mathrm{mean}}$ is the local mean of $DN(\lambda)_{\mathrm{high}}$ over a neighborhood, which is equivalent to the resolution of $DN(\lambda)_{\mathrm{low}}$. $DN(\lambda)_{\mathrm{low}}$ is the DN value of the MHS image upsampled to the simulated higher resolution, whereas $DN(\lambda)_{\mathrm{high}}$ is the DN value of the PAN image. It can be seen from (20) that low-resolution MHS images need to be upsampled to simulated higher resolution. Because the image is generally discrete, part of the information will be lost when upsampling, especially when the ratio of PAN to MHS image is large.

The proposed method defines the PAN decomposition coefficients $\rho_L^{(b)}$, which are calculated on the MHS resolution. Fig. 4 shows an example of the decomposition coefficients. Then, the PAN decomposition coefficients $\rho_L^{(b)}$ are upsampled to a PAN image resolution: $\rho^{(b)}$. The decomposition coefficients can maintain continuity while upsampling. Even if the ratio of PAN and MHS images is larger, less information will be lost

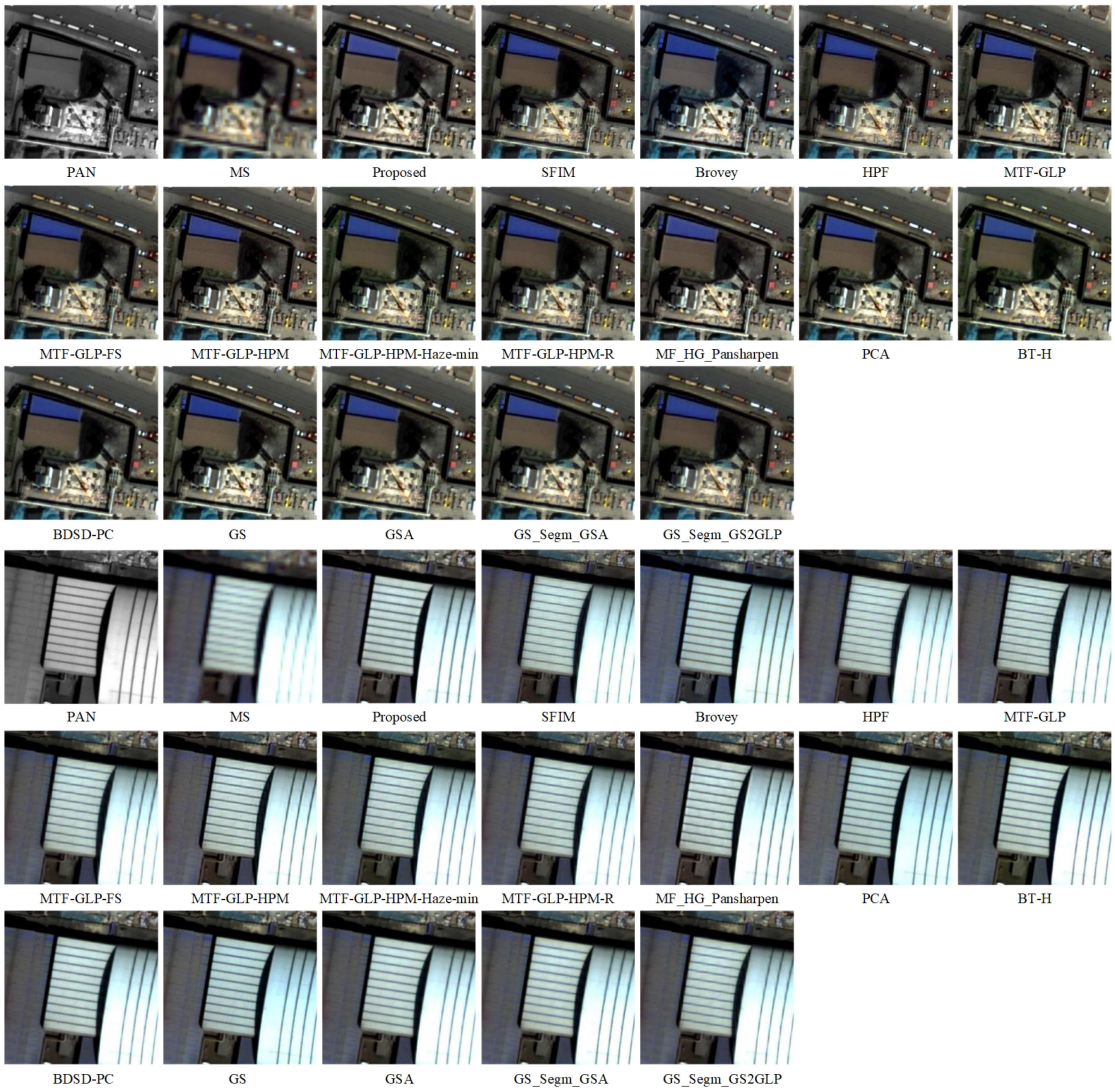

Fig. 3. Details of GF-7 color image with bands 3, 2, and 1 as RGB of different methods.

Fig. 4. PAN decomposition coefficients on MHS resolution.

during upsampling. This is an important factor for the proposed algorithm to still obtain better results when the ratio of PAN and MHS images is large.

2) Reduced-Resolution Assessment With Reference: This study assumes that the PAN image has the intensity of the MHS image. However, in fact, it is valid that the spectral range of PAN images does not include the spectral range of MHS images because this method can also regard PAN images as spatial information and the decomposition coefficients as color information. It is just that the color information is compressed by downsampling. Therefore, the algorithm in this article has good robustness to the correlation between PAN and MHS images. Even if the correlation between PAN and MHS images is low, it still has a good effect.

This study took the PAN image and midwave infrared (MIR) image of GF-4 as examples for testing. The spectral range of the PAN image is $0.45 - 0.90$ μm, whereas the spectral range of the MIR image is $3.5 - 4.1$ μm. Fig. 5 shows the MIR image sharpening result of GF-4. The correlation coefficients between

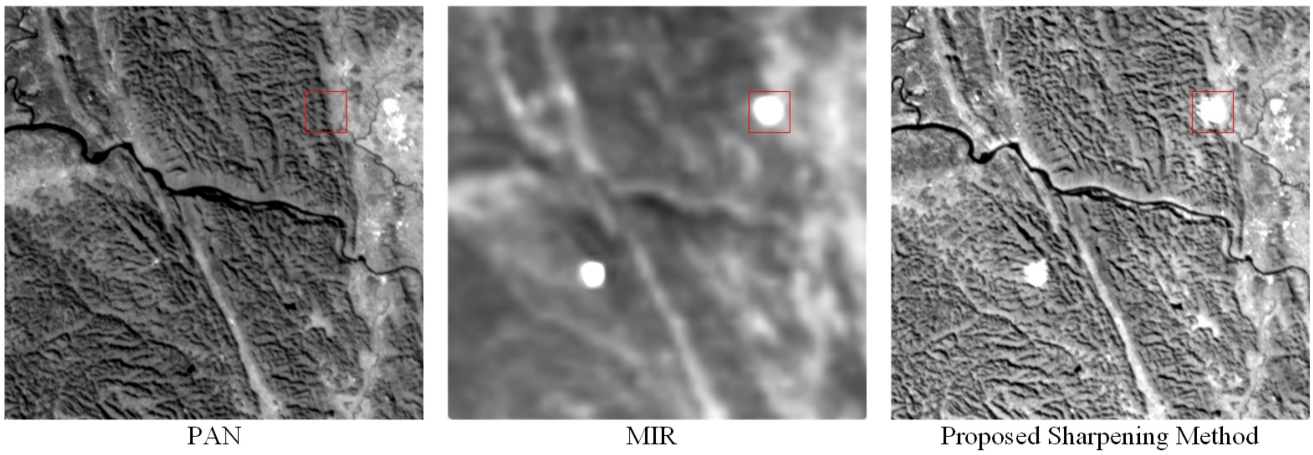

Fig. 5. MIR image sharpening for GF-4.

the PAN and MIR images are 0.3187, which is much lower than the correlation coefficients between general PN and MHS images. However, the algorithm in this article can still obtain better fusion results. Quantitative evaluation was performed by calculating $HQNR$, where D_S was 0.189, D_λ was 0.129, and $HQNR$ was 0.706, which indicated that both spatial information and spectral information were effectively preserved. In addition, unlike the CS method, the MRA method is generally not limited by the number of bands, and the method in this article also has such advantages. For the single-band fusion of the PAN and MIR images of GF-4, the CS method cannot be completed.

The results in this section show that the method in this article has a wide range of applications and a high computational efficiency. The principle is simple and easy to engineer. Combining with registration methods [52] can develop efficient and high-quality engineering applications. Related applications can be found at.[2] This study uses this program to test the sharpening of MSS images of different satellites and obtain good results, such as GF-DM, GF-2, and GF-6. This study also tested the sharpening of real HS images, sharpened the HS images of ZY-1E with the GF-7 PAN images, and achieved good results. The relevant results can be found in the Appendix.

3) Performance At Different Resolutions: To verify the performance under different resolutions, this study, respectively, calculates the results of the ratio $R \in 4, 8, 16, 32, 64$ and chooses the $RMSE$ index that best reflects the accuracy of the fusion method under the reference situation. Because the $RMSE$ of the fused image and the reference image is directly calculated, the smaller the value, the closer the value of the ground true image. It can be seen from Table IV that the $RMSE$ of the proposed method is slightly lower than that of the GS_Segm_GSA method for ratios of 4 and 8, and the proposed method has obvious advantages over the other methods for the other ratios. Compared with the HS image fusion methods Bayesian_Naive and HySure, it can establish a clear lead in different proportions.

The $RMSE$ of the proposed method gradually increases with the increase of the ratio, which indicates that it will lose part of the information as the ratio increases. In Fig. 6, it can be clearly seen that, as the proportion increases, although the spatial information is still better preserved, the color information is obviously lost. Because the method in this article was based on the decomposition of PAN images, it retained better spatial information. However, for the color information part, the algorithm in this article can only rely on the observed spectral information for interpolation. If the ratio is large, some color details will be lost.

To further illustrate the performance of the algorithm in this article under a large ratio, this study takes the case where the ratio is 64 as an example. In Fig. 7, the simulated observation PAN, HS, and fusion results of the proposed method are compared. It can be seen from the figure that most of the spatial information of the fusion result is preserved. However, the spectral information is considered to have a large difference in proportions, and part of the details are lost. However, it can retain the overall spectral effect. This shows that the algorithm in this article can perform well even at a large ratio of PAN and HS images.

All in all, the algorithm in this article performs well in image fusion, especially when the ratio of PAN and HS images is large,

TABLE IV
RMSE INDEX IN RATIO $R \in 4, 8, 16, 32, 64$ FOR ZY-1E IMAGE SHARPENING

Name \ ratio	4	8	16	32	64
GT	0	0	0	0	0
EXP	91.763	121.098	146.341	168.112	188.349
Proposed	43.160	55.448	**63.864**	**69.495**	**73.542**
SFIM	69.194	95.521	275.206	116.430	125.876
Brovey	50.840	69.591	87.404	106.345	130.254
HPF	62.227	80.205	94.155	107.092	125.729
MTF-GLP	49.647	61.815	102.498	373.014	412.677
MTF-GLP-FS	51.667	64.301	99.955	384.343	377.552
MTF-GLP-HPM	72.235	300.681	1733.013	523.038	587.848
MTF-GLP-HPM-Haze-min	54.620	535.072	108.061	576552.202	185.351
MTF-GLP-HPM-R	52.255	64.996	103.832	532.110	441.527
MF_HG_Pansharpen	67.642	70.692	88.334	88.429	108.670
PCA	51.031	67.374	84.464	103.520	127.847
BT-H	48.384	62.723	104.061	878033.356	183.757
BDSD-PC	44.478	53.548	179.677	552.744	598.143
GS	47.218	65.374	83.574	103.402	128.336
GSA	41.758	55.828	68.683	88.957	131.626
GS_Segm_GSA	**39.919**	**50.464**	85.661	357.837	262.644
GS_Segm_GS2GLP	53.830	68.111	96.828	237.006	211.357
Bayesian_Naive	73.234	81.639	77.054	74.359	76.111
HySure	45.186	62.062	71.741	87.922	93.332

[2][Online]. Available: https://github.com/whuxiegq/rsoneFusion

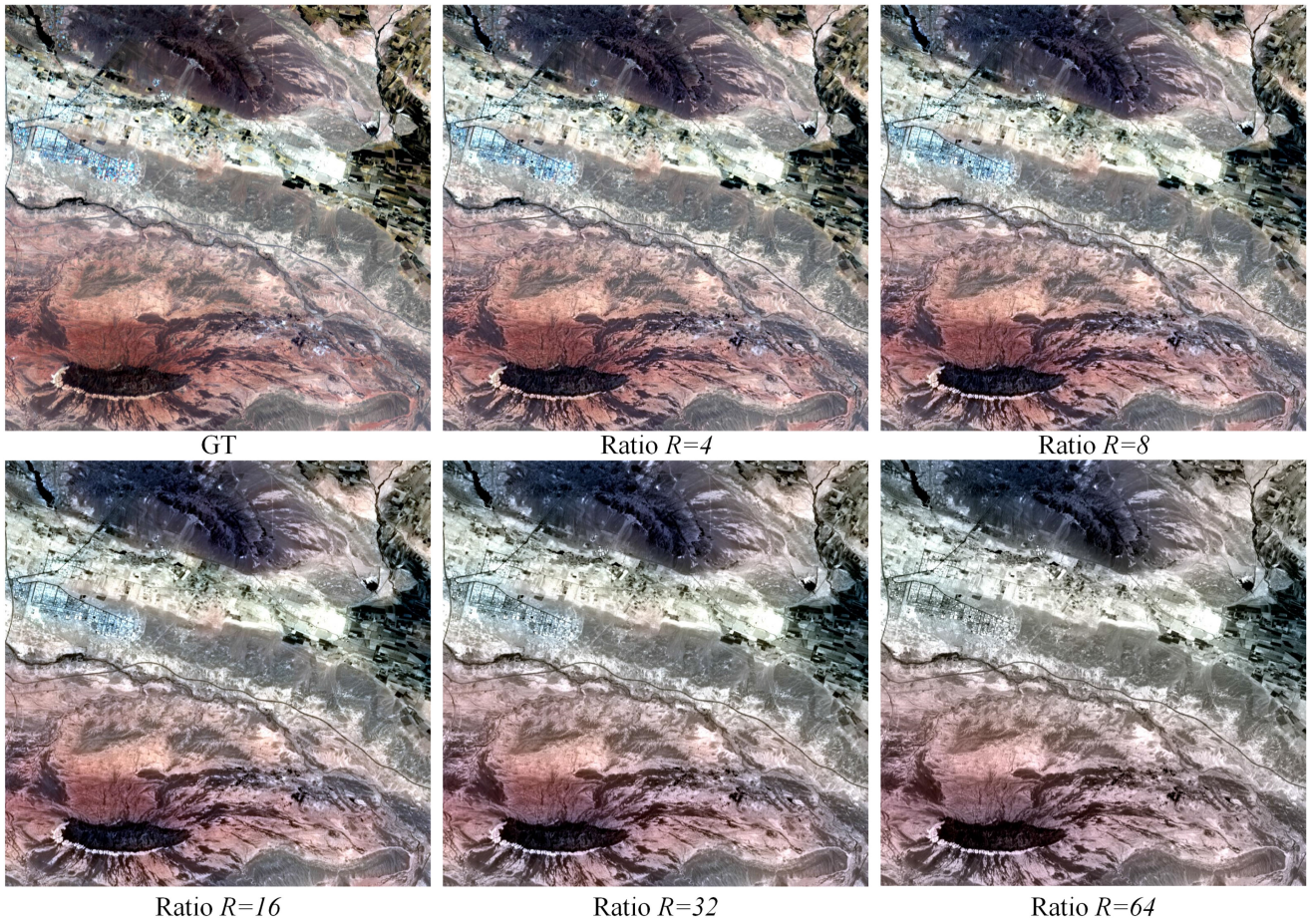

Fig. 6. ZY-1E color image with bands 25, 16, and 8 as RGB for different ratio of HS and GT images.

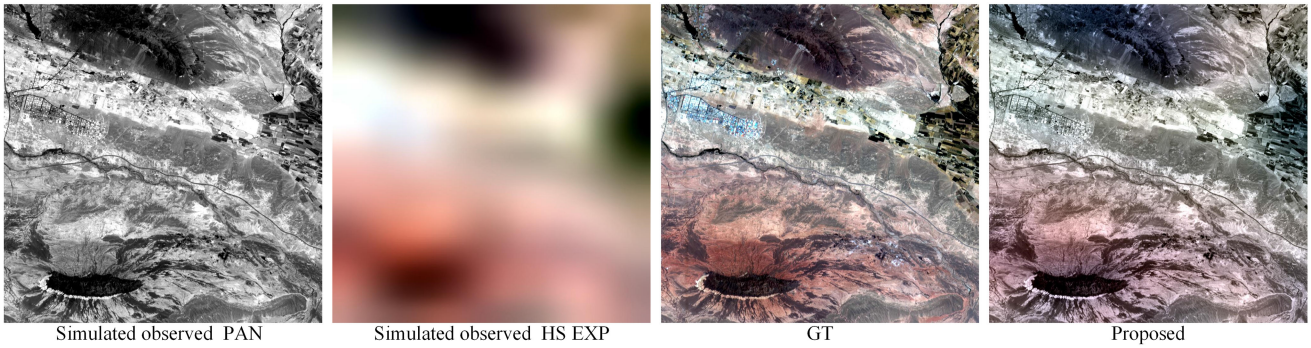

Fig. 7. ZY-1E color image with bands 25, 16, and 8 as RGB for ratio $R = 64$ for proposed fusion method.

and it has obvious advantages over the existing mainstream algorithms. Both subjective evaluation and objective evaluation can achieve good results.

4) Comparison With HPM Framework: The well-known high pass modulation (HPM) framework [53], [54] extracts high-frequency information from PAN images and injects them into MHS images. The high-frequency components of the PAN image are filtered out, and then the high-frequency information is extracted and injected into the low-resolution image by the ratio of the original PAN image and the filtered PAN image. The formula is expressed as follows:

$$\hat{\mathbf{M}} = \widetilde{\mathbf{M}} \bullet \frac{\mathbf{P}}{\widetilde{\mathbf{P}}}. \tag{19}$$

In the above formula, $\hat{\mathbf{M}}$ is the sharpened image, $\widetilde{\mathbf{M}}$ is the MHS image upsampled to the PAN image scale, P is the PAN image, and $\widetilde{\mathbf{P}}$ is the low-frequency component of the PAN image, which is prefiltered, downsampled, and upsampled.

TABLE V
COMPARISON BETWEEN HPM FRAMEWORK AND THE PROPOSED METHOD

Image	Method	D_λ	D_s	$HQNR$
GF-7	HPM	**0.006**	0.051	0.942
	Proposed	0.022	**0.029**	**0.950**
GF-DM	HPM	**0.012**	0.035	0.953
	Proposed	0.017	**0.027**	**0.955**
GF-2	HPM	**0.013**	0.074	0.913
	Proposed	0.019	**0.057**	**0.924**
GF-6	HPM	**0.043**	0.084	0.876
	Proposed	0.052	**0.074**	**0.878**

In this article, it is assumed that an image of different scales has only high-frequency spatial differences and no low-frequency spectral differences. Therefore, the spectral decomposition coefficients on different scales are the same.

The high frequency components of the PAN image were filtered out and down-sampled to the MHS image scale, the down-sampled PAN image was spectrally decomposed by ratio, and then the decomposition coefficients were up-sampled to the PAN image scale to decompose the original PAN image. Ideally, the high frequency components of the sharpened image should be consistent with the PAN image, and the formula can be written as follows:

$$\hat{\mathbf{M}} = P \bullet \left(\frac{\mathbf{P_L}}{\mathbf{M}} \uparrow \right). \tag{20}$$

In the above formula, $\hat{\mathbf{M}}$ is the sharpened image, P is the PAN image, $\mathbf{P_L}$ is a prefiltered and down-sampled PAN image on MHS scale, M is the MHS image, and $\uparrow$ means upsampling.

From the comparison of the formulas, it can be seen that the main difference between the method in this paper and the HPM framework is whether the ratio operation is performed at the PAN scale or the MHS scale. This article assumes that if all the redundant high-frequency information in the PAN image was filtered out and down-sampled, the down-sampled PAN image had the same spatial detail information as the MHS image. At this time, the main difference in the image was the spectral information, which can used ratio method decomposes the spectrum without changing the spatial details. This design preserves spatial details to the greatest extent possible.

In order to verify the effect of the method in this article, this article controlled other variables to compare with the HPM framework, and the difference was only whether the ratio calculation was performed on PAN scale or MHS scale. As shown in Table I, data from different satellites were selected for full-resolution assessment with no reference. The data (including the appendix) were used in this article.

As can be seen from Table V, the $HQNR$ of the proposed method is better than that of the HPM framework, and D_s is better than HPM, but D_λ is worse than HPM. As analyzed above, the proposed method preserves the spatial details better because the proposed method decomposes the PAN image spectrally without changing the spatial detail information. While the HPM method injects spatial detail information into the low-frequency spectrum, its spectral preservation ability is better than the proposed method.

In the images with richer spatial details, the advantages of the method in this article are more obvious, and fewer spatial details are lost. For example, for the GF-7 and GF-2 data in Table I, the image is located in an urban area with rich spatial details, and the $HQNR$ of the proposed method is significantly higher than that of the HPM method.

V. CONCLUSION

This article proposes an MS and HS image pansharpening method: SFPSD. The method has a wide range of applications and a high computational efficiency and is suitable for the sharpening of not only traditional MS images, but also HS images and single-band MIR images. In addition, good results have been obtained for the objective evaluation index with and without reference.

The method in this article uses the decomposition coefficients to decompose the PAN image into a high-spatial-resolution MHS image. It can obtain a fused image with both high spatial and spectral resolutions. The decomposition coefficients are calculated using the MHS image and the PAN blurred downsampled image and is then upsampled to the resolution of the PAN image, which decomposes the PAN image into a high-resolution MHS image. This study separately evaluates the reduced-resolution assessment of HS image sharpening with reference and the full-resolution assessment of MS image sharpening without reference. Based on the results, when compared with 18 common methods, the method in this article obtains the best results regardless of subjective or objective evaluation. Moreover, when the ratio of PAN and MHS images is larger, the effect is better than the others. In the reduced-resolution assessment with reference, the $RMSE$ index of the method in this article can reach about 70, even when the ratio of PAN and MHS images is 64. In the full-resolution assessment with no reference, the $HQNR$ index of this method is 0.949931, which is also better than those of the other methods. In addition, the decomposition coefficients of the method in this article are continuous and robust to PAN and MHS images.

The principle of the method in this article is clear, the calculation efficiency is high, and the engineering is easy. The related MATLAB source code and engineering program can be found at.[3] The engineering procedure in this article has been validated for MS image sharpening of multiple Chinese satellites and achieved good results. This study also sharpened the ZY-1E HS image with the GF-7 PAN image and obtained good results too.

APPENDIX

See Appendix Figs. 8 to 11.

[3][Online]. Available: https://github.com/whuxiegq/rsoneFusion

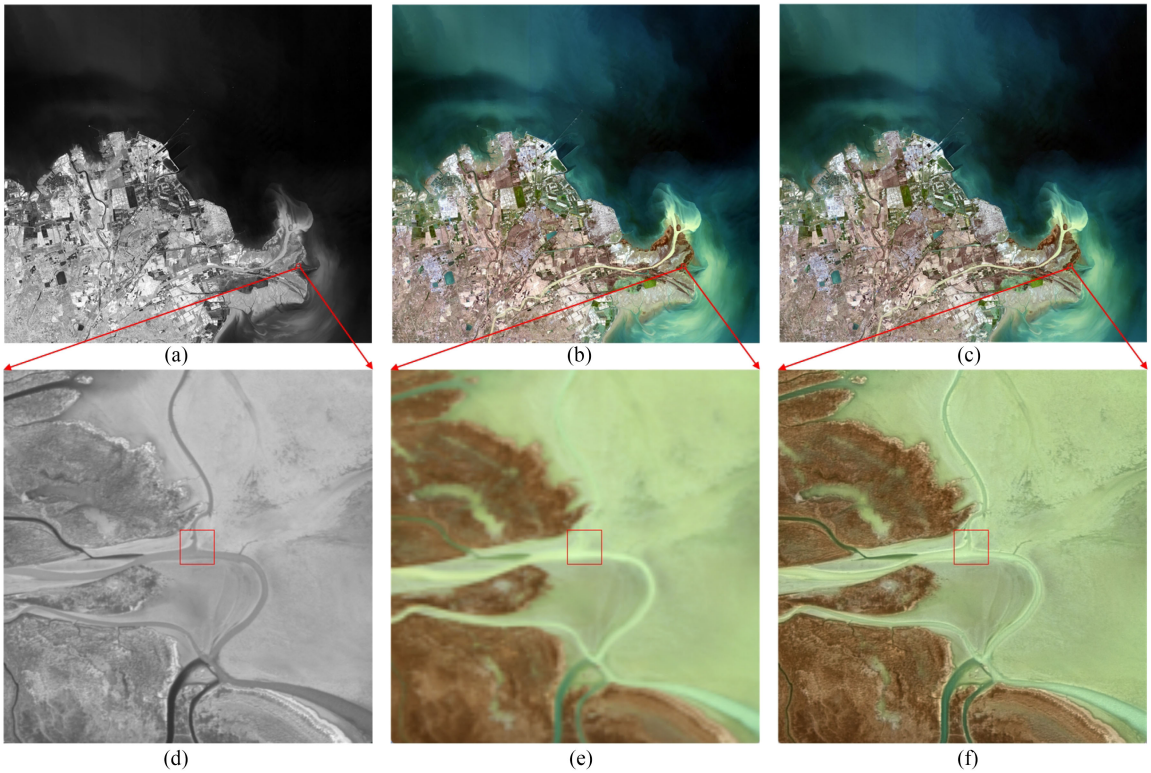

Fig. 8. Image sharpening for GF-DM. (a) GF-DM PAN. (b) GF-DM MS. (c) Proposed sharpening image. (d) Detail of GF-DM PAN. (e) Detail of GF-DM MS. (f) Detail of proposed sharpening image.

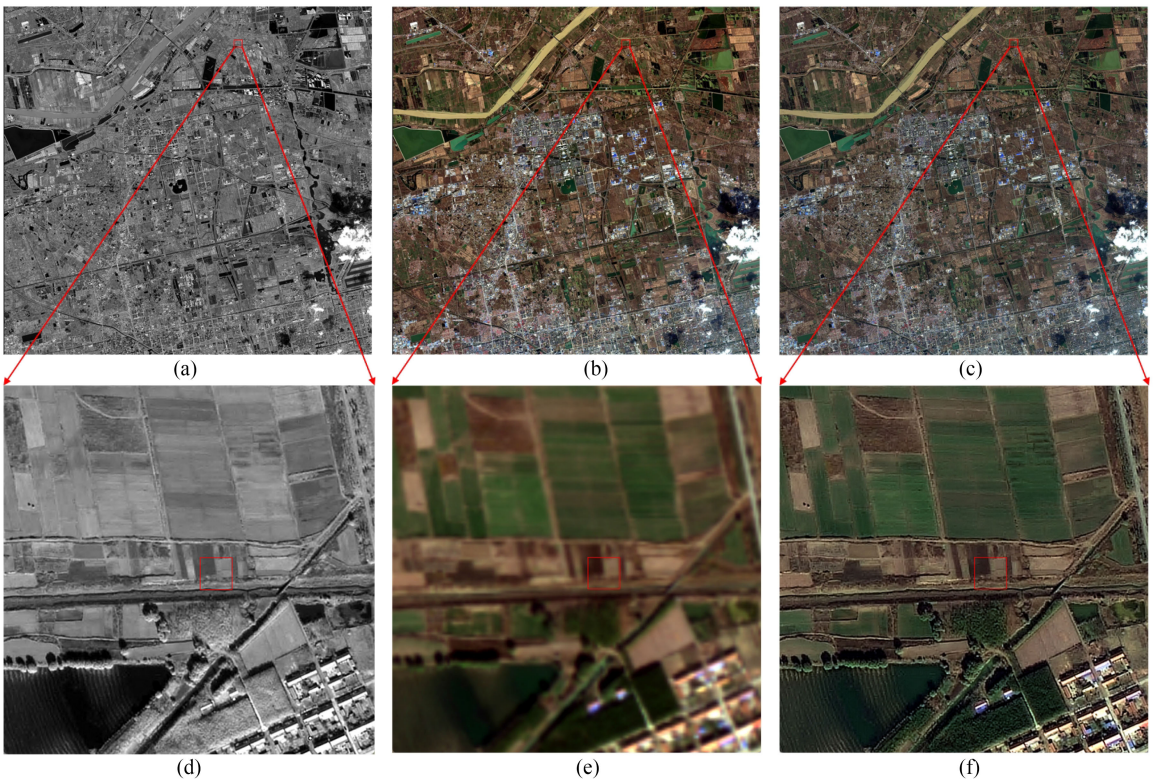

Fig. 9. Image sharpening for GF-2. (a) GF-2 PAN. (b) GF-2 MS. (c) Proposed sharpening image. (d) Detail of GF-2 PAN. (e) Detail of GF-2 MS. (f) Detail of proposed sharpening image.

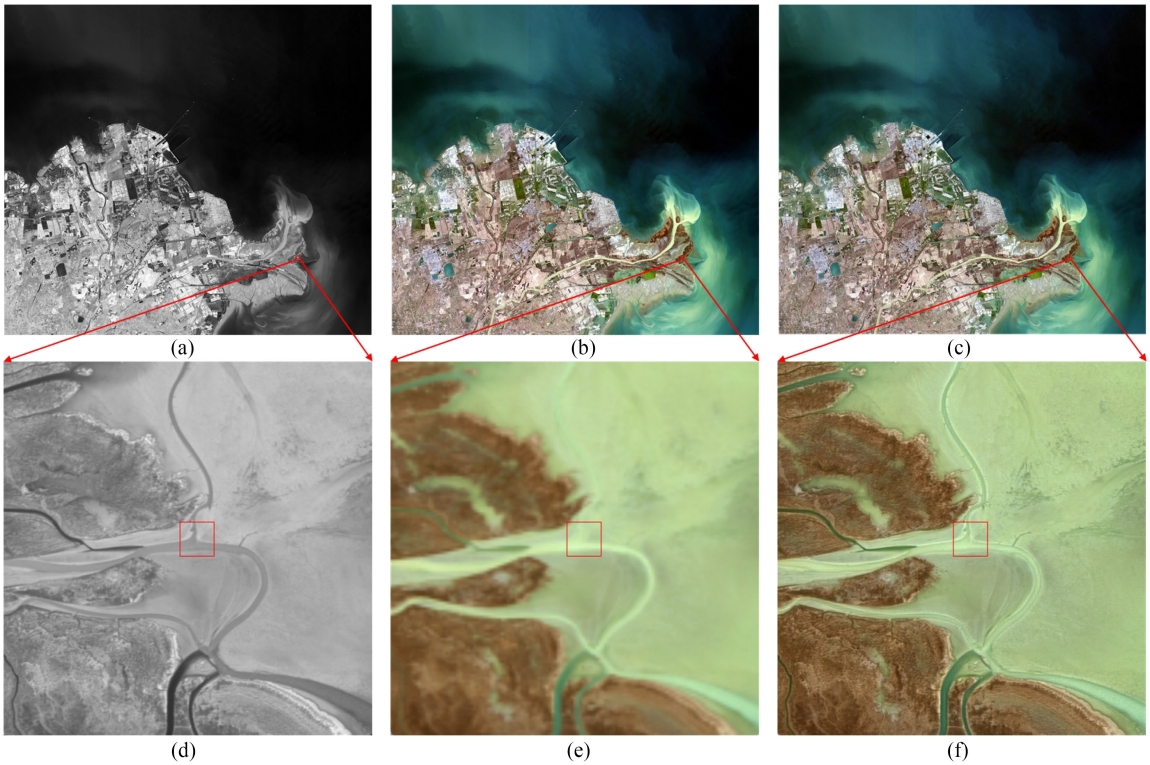

Fig. 10. Image sharpening for GF-6. (a) GF-6 PAN. (b) GF-6 MS. (c) Proposed sharpening image. (d) Detail of GF-6 PAN. (e) Detail of GF-6 MS. (f) Detail of proposed sharpening image.

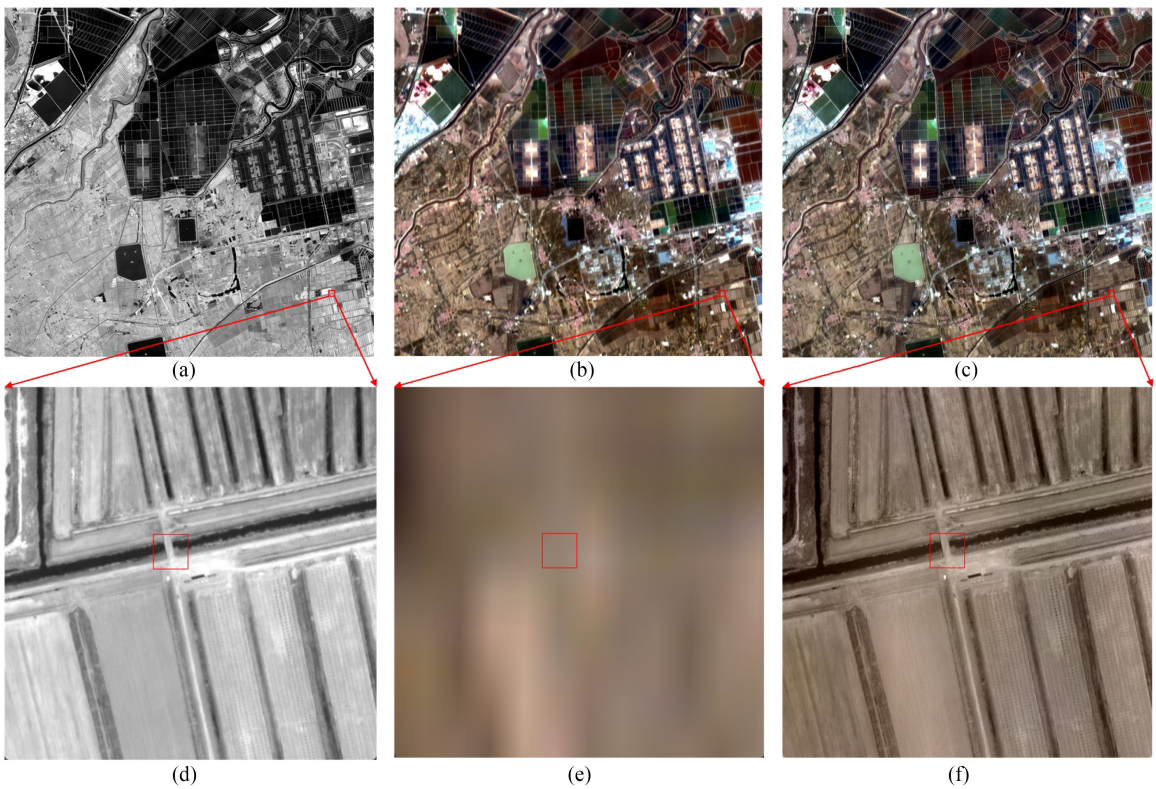

Fig. 11. Image sharpening for ZY-1E HS by GF-7 PAN. (a) GF-7 PAN. (b) ZY-1E HS. (c) Proposed sharpening image. (d) Detail of GF-7 PAN. (e) Detail of ZY-1E HS. (f) Detail of proposed sharpening image.

ACKNOWLEDGMENT

The authors would like to thank the China Centre For Resources Satellite Data and Application for providing the data used in this article.

REFERENCES

[1] H. Ghassemian, "A review of remote sensing image fusion methods," *Inf. Fusion*, vol. 32, pp. 75–89, Nov. 2016.

[2] G. Vivone *et al.*, "A new benchmark based on recent advances in multispectral pansharpening," *IEEE Geosci. Remote Sens. Mag.*, vol. 9, no. 1, pp. 53–81, Mar. 2021.

[3] F. Dadrass Javan, F. Samadzadegan, S. Mehravar, A. Toosi, R. Khatami, and A. Stein, "A review of image fusion techniques for pan-sharpening of high-resolution satellite imagery," *ISPRS J. Photogramm. Remote Sens.*, vol. 171, pp. 101–117, Jan. 2021.

[4] L. He, J. Zhu, J. Li, A. Plaza, J. Chanussot, and Z. Yu, "Cnn-based hyperspectral pansharpening with arbitrary resolution," *IEEE Trans. Geosci. Remote Sens.*, vol. 60, pp. 1–21, 2022, Dec., doi: 10.1109/TGRS.2021.3132997.

[5] L. He *et al.*, "Pansharpening via detail injection based convolutional neural networks," *IEEE J. Sel. Topics Appl. Earth Observ. Remote Sens.*, vol. 12, no. 4, pp. 1188–1204, Apr. 2019.

[6] C. Jin, L.-J. Deng, T.-Z. Huang, and G. Vivone, "Laplacian pyramid networks: A new approach for multispectral pansharpening," *Inf. Fusion*, vol. 78, pp. 158–170, 2022.

[7] G. Vivone *et al.*, "A critical comparison among pansharpening algorithms," *IEEE Trans. Geosci. Remote Sens.*, vol. 53, no. 5, pp. 2565–2586, May 2014.

[8] L. Alparone, L. Wald, J. Chanussot, C. Thomas, P. Gamba, and L. M. Bruce, "Comparison of pansharpening algorithms: Outcome of the 2006 GRS-S data-fusion contest," *IEEE Trans. Geosci. Remote Sens.*, vol. 45, no. 10, pp. 3012–3021, Oct. 2007.

[9] P. Kwarteng and A. Chavez, "Extracting spectral contrast in landsat thematic mapper image data using selective principal component analysis," *Photogramm. Eng. Remote Sens*, vol. 55, no. 1, pp. 339–348, 1989.

[10] V. K. Shettigara, "A generalized component substitution technique for spatial enhancement of multispectral images using a higher resolution data set," *Photogrammetric Eng. Remote Sens.*, vol. 58, no. 5, pp. 561–567, 1992.

[11] V. P. Shah, N. H. Younan, and R. L. King, "An efficient pan-sharpening method via a combined adaptive PCA approach and contourlets," *IEEE Trans. Geosci. Remote Sens.*, vol. 46, no. 5, pp. 1323–1335, Apr. 2008.

[12] A. R. Gillespie, A. B. Kahle, and R. E. Walker, "Color enhancement of highly correlated images. II. channel ratio and 'chromaticity' transformation techniques," *Remote Sens. Environ.*, vol. 22, no. 3, pp. 343–365, Aug. 1987.

[13] T.-M. Tu, S.-C. Su, H.-C. Shyu, and P. S. Huang, "A new look at IHS-like image fusion methods," *Inf. Fusion*, vol. 2, no. 3, pp. 177–186, Sep. 2001.

[14] B. Aiazzi, S. Baronti, M. Selva, and L. Alparone, "Enhanced Gram-Schmidt spectral sharpening based on multivariate regression of MS and pan data," in *Proc. IEEE Int. Symp. Geosci. Remote Sens.*, 2006, pp. 3806–3809.

[15] K. Zhang, F. Zhang, Z. Feng, J. Sun, and Q. Wu, "Fusion of panchromatic and multispectral images using multiscale convolution sparse decomposition," *IEEE J. Sel. Topics Appl. Earth Observ. Remote Sens.*, vol. 14, pp. 426–439, Dec. 2021, doi: 10.1109/JSTARS.2020.3043521.

[16] M. M. Khan, J. Chanussot, L. Condat, and A. Montanvert, "Indusion: Fusion of multispectral and panchromatic images using the induction scaling technique," *IEEE Geosci. Remote Sens. Lett.*, vol. 5, no. 1, pp. 98–102, Jan. 2008.

[17] J. Liu, "Smoothing filter-based intensity modulation: A spectral preserve image fusion technique for improving spatial details," *Int. J. Remote Sens.*, vol. 21, no. 18, pp. 3461–3472, 2000.

[18] P. Chavez, S. C. Sides, and J. A. Anderson, "Comparison of three different methods to merge multiresolution and multispectral data: Landsat TM and SPOT panchromatic," *Photogrammetric Eng. Remote Sens.*, vol. 57, no. 3, pp. 295–303, 1991.

[19] B. Aiazzi, L. Alparone, S. Baronti, A. Garzelli, and M. Selva, "MTF-tailored multiscale fusion of high-resolution MS and pan imagery," *Photogrammetric Eng. Remote Sens.*, vol. 72, no. 5, pp. 591–596, 2006.

[20] R. Restaino, G. Vivone, M. Dalla Mura, and J. Chanussot, "Fusion of multispectral and panchromatic images based on morphological operators," *IEEE Trans. Image Process.*, vol. 25, no. 6, pp. 2882–2895, Jun. 2016, doi: 10.1109/TIP.2016.2556944.

[21] T. A. Wilson, S. K. Rogers, and M. Kabrisky, "Perceptual-based image fusion for hyperspectral data," *IEEE Trans. Geosci. Remote Sens.*, vol. 35, no. 4, pp. 1007–1017, 1997, doi: 10.1109/36.602543.

[22] L. Alparone, V. Cappellini, L. Mortelli, B. Aiazzi, S. Baronti, and R. Carlà, "A pyramid-based approach to multisensor image data fusion with preservation of spectral signatures," *Future Trends Remote Sens.*, pp. 418–426, 1998.

[23] L. He, J. Zhu, J. Li, D. Meng, J. Chanussot, and A. Plaza, "Spectral-fidelity convolutional neural networks for hyperspectral pansharpening," *IEEE J. Sel. Topics Appl. Earth Observ. Remote Sens.*, vol. 13, pp. 5898–5914, Sep. 2020, doi: 10.1109/JSTARS.2020.3025040.

[24] L. Liu *et al.*, "Shallow and spectral-discrimination-based detail injection for multispectral imagery pan-sharpening," *IEEE J. Sel. Topics Appl. Earth Observ. Remote Sens.*, vol. 13, pp. 1772–1783, Mar. 2020, doi: 10.1109/JSTARS.2020.2981695.

[25] Q. Yuan, Y. Wei, X. Meng, H. Shen, and L. Zhang, "A multiscale and multidepth convolutional neural network for remote sensing imagery pan-sharpening," *IEEE J. Sel. Topics Appl. Earth Observ. Remote Sens.*, vol. 11, no. 3, pp. 978–989, Mar. 2018.

[26] Q. Liu, H. Zhou, Q. Xu, X. Liu, and Y. Wang, "PSGAN: A generative adversarial network for remote sensing image pan-sharpening," in *Proc. IEEE Trans. Geosci. Remote Sens.*, 2020, pp. 1–16.

[27] J. Ma, W. Yu, C. Chen, P. Liang, X. Guo, and J. Jiang, "Pan-GAN: An unsupervised pan-sharpening method for remote sensing image fusion," *Inf. Fusion*, vol. 62, pp. 110–120, Oct. 2020.

[28] J. Xiao, J. Li, Q. Yuan, M. Jiang, and L. Zhang, "Physics-based GAN with iterative refinement unit for hyperspectral and multispectral image fusion," *IEEE J. Sel. Topics Appl. Earth Observ. Remote Sens.*, vol. 14, pp. 6827–6841, May 2021, doi: 10.1109/JSTARS.2021.3075727.

[29] Y. Xing, S. Yang, Z. Feng, and L. Jiao, "Dual-collaborative fusion model for multispectral and panchromatic image fusion," *IEEE Trans. Geosci. Remote Sens.*, vol. 60, pp. 1–15, 2022, doi: 10.1109/TGRS.2020.3036625.

[30] Q. Wei, N. Dobigeon, and J.-Y. Tourneret, "Bayesian fusion of multi-band images," *IEEE J. Sel. Topics Signal Process.*, vol. 9, no. 6, pp. 1117–1127, Sep. 2015.

[31] M. Simões, J. Bioucas-Dias, L. B. Almeida, and J. Chanussot, "Hyperspectral image superresolution: An edge-preserving convex formulation," in *Proc. IEEE Int. Conf. Image Process.*, 2014, pp. 4166–4170.

[32] M. Simões, J. Bioucas-Dias, L. B. Almeida, and J. Chanussot, "A convex formulation for hyperspectral image superresolution via subspace-based regularization," *IEEE Trans. Geosci. Remote Sens.*, vol. 53, no. 6, pp. 3373–3388, Jun. 2015.

[33] M. M. Khan, L. Alparone, and J. Chanussot, "Pansharpening quality assessment using the modulation transfer functions of instruments," *IEEE Trans. Geosci. Remote Sen.*, vol. 47, no. 11, pp. 3880–3891, Nov. 2009.

[34] Z. Wang and A. Bovik, "A universal image quality index," *IEEE Signal Process. Lett.*, vol. 9, no. 3, pp. 81–84, Mar. 2002.

[35] L. Alparone, S. Baronti, A. Garzelli, and F. Nencini, "A global quality measurement of pan-sharpened multispectral imagery," *IEEE Geosci. Remote Sens. Lett.*, vol. 1, no. 4, pp. 313–317, Oct. 2004.

[36] A. Garzelli and F. Nencini, "Hypercomplex quality assessment of multi/hyperspectral images," *IEEE Geosci. Remote Sens. Lett.*, vol. 6, no. 4, pp. 662–665, Oct. 2009.

[37] B. Aiazzi, L. Alparone, S. Baronti, R. Carlà, A. Garzelli, and L. Santurri, "Full-scale assessment of pansharpening methods and data products," *Image Signal Process. Remote Sens. XX, Int. Soc. Opt. Photon.*, vol. 9244, 2014, Art. no. 924402.

[38] G. Vivone, M. Dalla Mura, A. Garzelli, and F. Pacifici, "A benchmarking protocol for pansharpening: Dataset, preprocessing, and quality assessment," *IEEE J. Sel. Topics Appl. Earth Observ. Remote Sens.*, vol. 14, pp. 6102–6118, 2021, doi: 10.1109/JSTARS.2021.3086877.

[39] N. Yokoya, C. Grohnfeldt, and J. Chanussot, "Hyperspectral and multispectral data fusion: A comparative review of the recent literature," *IEEE Geosci. Remote Sens. Mag.*, vol. 5, no. 2, pp. 29–56, Jun. 2017.

[40] L. Loncan *et al.*, "Hyperspectral pansharpening: A review," *IEEE Geosci. remote Sens. Mag.*, vol. 3, no. 3, pp. 27–46, Sep. 2015.

[41] "Resize image - MATLAB imresize - MathWorks China," [Online]. Available: https://ww2.mathworks.cn/help/matlab/ref/imresize.html?lang=en

[42] B. Aiazzi, L. Alparone, S. Baronti, and A. Garzelli, "Context-driven fusion of high spatial and spectral resolution images based on oversampled multiresolution analysis," *IEEE Trans. Geosci. Remote Sens.*, vol. 40, no. 10, pp. 2300–2312, Oct. 2002.
[43] G. Vivone, R. Restaino, and J. Chanussot, "Full scale regression-based injection coefficients for panchromatic sharpening," *IEEE Trans. Image Process.*, vol. 27, no. 7, pp. 3418–3431, Jul. 2018.
[44] B. Aiazzi, L. Alparone, S. Baronti, A. Garzelli, and M. Selva, "An MTF-based spectral distortion minimizing model for pan-sharpening of very high resolution multispectral images of urban areas," in *Proc. 2nd GRSS/ISPRS Joint Workshop Remote Sens. Data Fusion Over Urban Areas*, 2003, pp. 90–94.
[45] S. Lolli, L. Alparone, A. Garzelli, and G. Vivone, "Haze correction for contrast-based multispectral pansharpening," *IEEE Geosci. Remote Sens. Lett.*, vol. 14, no. 12, pp. 2255–2259, Dec. 2017.
[46] G. Vivone, R. Restaino, and J. Chanussot, "A regression-based high-pass modulation pansharpening approach," *IEEE Trans. Geosci. Remote Sens.*, vol. 56, no. 2, pp. 984–996, Feb. 2018.
[47] G. Vivone, "Robust band-dependent spatial-detail approaches for panchromatic sharpening," *IEEE Trans. Geosci. Remote Sens.*, vol. 57, no. 9, pp. 6421–6433, Sep. 2019.
[48] B. Aiazzi, S. Baronti, and M. Selva, "Improving component substitution pansharpening through multivariate regression of MS pan data," *IEEE Trans. Geosci. Remote Sens.*, vol. 45, no. 10, pp. 3230–3239, Oct. 2007.
[49] R. Restaino, M. Dalla Mura, G. Vivone, and J. Chanussot, "Context-adaptive pansharpening based on image segmentation," *IEEE Trans. Geosci. Remote Sens.*, vol. 55, no. 2, pp. 753–766, Feb. 2017.
[50] S. Baronti, B. Aiazzi, M. Selva, A. Garzelli, and L. Alparone, "A theoretical analysis of the effects of aliasing and misregistration on pansharpened imagery," *IEEE J. Sel. Topics Signal Process.*, vol. 5, no. 3, pp. 446–453, Jun. 2011.
[51] S. Yang, K. Zhang, and M. Wang, "Learning low-rank decomposition for pan-sharpening with spatial-spectral offsets," *IEEE Trans. Neural Netw. Learn. Syst.*, vol. 29, no. 8, pp. 3647–3657, Aug. 2018.
[52] G. Xie, M. Wang, Z. Zhang, S. Xiang, and L. He, "Near real-time automatic sub-pixel registration of panchromatic and multispectral images for pan-sharpening," *Remote Sens.*, vol. 13, no. 18, Jan. 2021, Art. no. 3674.
[53] J. Lee and C. Lee, "Fast and efficient panchromatic sharpening," *IEEE Trans. Geosci. Remote Sens.*, vol. 48, no. 1, pp. 155–163, Jan. 2010.
[54] G. Vivone, R. Restaino, M. Dalla Mura, G. Licciardi, and J. Chanussot, "Contrast and error-based fusion schemes for multispectral image pan-sharpening," *IEEE Geosci. Remote Sens. Lett.*, vol. 11, no. 5, pp. 930–934, May 2014.
[55] Y. Xing, Y. Zhang, S. Yang, and Y. Zhang, "Hyperspectral and multispectral image fusion via variational tensor subspace decomposition," *IEEE Geosci. Remote Sens. Lett.*, vol. 19, pp. 1–5, 2021, doi: 10.1109/LGRS.2021.3094558.
[56] W. Carper, T. Lillesand, and R. Kiefer, "The use of intensity-hue-saturation transformations for merging SPOT panchromatic and multispectral image data," *Photogrammetric Eng. remote Sens.*, vol. 56, no. 4, pp. 459–467, 1990.
[57] X. Otazu, M. Gonzalez-Audicana, O. Fors, and J. Nunez, "Introduction of sensor spectral response into image fusion methods. application to wavelet-based methods," *IEEE Trans. Geosci. Remote Sens.*, vol. 43, no. 10, pp. 2376–2385, Oct. 2005.
[58] Y. Zhang, "A new automatic approach for effectively fusing landsat 7 as well as IKONOS images," *IEEE Int. Geosci. Remote Sens. Symp.*, vol. 4, pp. 2429–2431, 2002, doi: 10.1109/IGARSS.2002.1026567.
[59] L. He, M. Wang, Y. Zhu, X. Chang, and X. Feng, "Image fusion for high-resolution optical satellites based on panchromatic spectral decomposition," *Sensors*, vol. 19, no. 11,, 2019, Art. no. 2619.
[60] D. G. Lowe, "Distinctive image features from scale-invariant keypoints," *Int. J. Comput. Vis.*, vol. 60, no. 2, pp. 91–110, 2004.

Mi Wang received the B.Sc., M.Sc., and Ph.D. degrees from Wuhan University, Wuhan, China, in 1997, 1999, and 2001, respectively, all in photogrammetry and remote sensing.

Since 2008, he has been a Professor with the State Key Laboratory of Information Engineering in Surveying, Mapping, and Remote Sensing, Wuhan University. His research interests include the measurable seamless stereo orthoimage databases, geographic information systems (GIS), and the integration global navigation satellite system, remote sensing, and GIS.

Guangqi Xie (Graduate Student Member, IEEE) received the M.Sc. degrees in remote sensing of resources and environment from the China University of Geosciences, Wuhan, China, in 2018. He is currently working toward the Ph.D. degree in photogrammetry and remote sensing with the State Key Laboratory of Information Engineering in Surveying, Mapping, and Remote Sensing, Wuhan University, Wuhan, China.

His research interest includes image matching and registration, pansharpening, and image super-resolution.

Zhiqi Zhang received the B.Sc. degree in geographic information system from Huazhong Agricultural University, Wuhan, China, in 2006, the B.Eng. degree in computer science and technology from the Huazhong University of Science and Technology, Wuhan, China, in 2006, the M.Eng. degree in computer technology from Wuhan University, Wuhan, China in 2015, and the Ph.D. degree in photogrammetry and remote sensing from Wuhan University, in 2018.

He is currently an Associate Professor with the School of Computer Science, Hubei University of Technology. His research interests include system architecture, algorithm optimization, AI and high performance processing of remote sensing.

Shao Xiang is currently working toward the Ph.D. degree in photogrammetry and remote sensing with Wuhan University, Wuhan, China.

His research interests include artificial intelligence, pattern recognition, remote sensing image processing, and information extraction.

Yan Wang received the B.Eng. degree in photogrammetry and remote sensing, in 2005.

Since 2017, she has been a Senior Engineer with the Institute of Beijing Remote Sensing Information. Her research interests include high precision remote sensing image processing and application.

Yingdong Pi received the B.Eng., M.Sc., and Ph.D. degrees in photogrammetry and remote sensing from Wuhan University, Wuhan, China, in 2014, 2017, and 2021, respectively.

He is currently a Postdoctoral Fellow of State Key Laboratory of Information Engineering in Surveying, Mapping, and Remote Sensing, Wuhan University. His research interests include high precision remote sensing image processing and deep space detection.